Lognormal-like statistics of a stochastic squeeze process

Dekel Shapira and Doron Cohen*

Department of Physics, Ben-Gurion University of the Negev, Beer-Sheva 84105, Israel

(Received 5 January 2017; revised manuscript received 1 October 2017; published 25 October 2017)

We analyze the full statistics of a stochastic squeeze process. The model's two parameters are the bare stretching rate w and the angular diffusion coefficient D. We carry out an exact analysis to determine the drift and the diffusion coefficient of $\log(r)$, where r is the radial coordinate. The results go beyond the heuristic lognormal description that is implied by the central limit theorem. Contrary to the common "quantum Zeno" approximation, the radial diffusion is not simply $D_r = (1/8)w^2/D$ but has a nonmonotonic dependence on w/D. Furthermore, the calculation of the radial moments is dominated by the far non-Gaussian tails of the $\log(r)$ distribution.

DOI: 10.1103/PhysRevE.96.042152

I. INTRODUCTION

In this paper we analyze the full statistics of a physically motivated stochastic squeeze process that is described by the Langevin (Stratonovich) equation,

$$\dot{x} = wx - \omega(t)y, \quad \dot{y} = -wy + \omega(t)x, \tag{1}$$

where the rotation frequency $\omega(t)$ is a zero-mean white noise with fluctuations:

$$\langle \omega(t')\omega(t'')\rangle = 2D\delta(t' - t''). \tag{2}$$

Accordingly the model has two parameters: the angular diffusion coefficient D of the polar phase and the bare stretching rate w of the radial coordinate $r = \sqrt{x^2 + y^2}$. In a physical context the noise arises due to the interaction with environmental degrees of freedom, typically modeled as a harmonic bath of "phonons." Hence we can assume for it a Gaussian-like distribution with bounded moments. The white noise assumption means that the correlation time is very short, hence the Stratonovich interpretation of Eq. (1) is in order, as argued, for example, by Van Kampen [1].

The squeeze operation is of interest in many fields of science and engineering, but our main motivation originates from the quantum mechanical arena, where it is known as parametric amplification. In particular, it describes the dynamics of a bosonic Josephson junction (BJJ) given that all the particles are initially condensed in the upper orbital. This preparation is *unstable* [2,3], but it can be stabilized by introducing frequent *measurements* or by introducing *noise*. This is the so-called "quantum Zeno effect" (QZE) [4–8]. The manifestation of the QZE in the BJJ context was first considered in Ref. [9] and [10] and later in Ref. [11].

The main idea of the QZE is usually explained as follows: The very short-time decay of an initial preparation due to constant perturbation is described by the survival probability $\mathcal{P}(t) = 1 - (vt)^2$, where v is determined by pertinent couplings to the other eigenstates; Dividing the evolution into τ steps and assuming a projective measurement at the end of each step one obtains

$$\mathcal{P}(t) \approx [\mathcal{P}(\tau)]^{t/\tau} \approx [1 - (v\tau)^2]^{t/\tau} \approx \exp[-(v^2\tau)t].$$

The common phrasing is that frequent measurements (small τ) slow down the decay process due to repeated "collapse" of the wave function. Optionally, one considers a system that is coupled to the environment. Such an interaction is formally similar to a continuous measurement process, which is characterized by a dephasing time τ. In the latter case the phrasing is that the introduction of "noise" leads to the slowdown of the decay process. Contrary to simple intuition, stronger noise leads to slower decay.

At this point one might get the impression that the QZE is a novel "quantum" effect, which has to do with mysterious collapses, and that this effect is not expected to arise in a "classical" reality. This conclusion is in fact wrong: Whenever the system of interest has a meaningful classical limit, the same Zeno effect arises also in the classical analysis. This point is emphasized in Ref. [11] in the context of the BJJ. It has been realized that the QZE is the outcome of the classical dynamics that is generated by Eq. (1), where the (x,y) are local canonical conjugate coordinates in the vicinity of a hyperbolic (unstable) fixed point in phase space. The essence of the QZE in this context is the observation that the introduction of the noise via the phase variable leads to a slowdown of the radial spreading. For strong noise [large D in Eq. (2)], the radial spreading due to w is inhibited. Using quantum terminology this translates to suppression of the decoherence process.

From a pedagogical point of view it is useful to note that the dynamics of the BJJ is formally similar to that of a mathematical pendulum. Condensation of all the particles in the upper orbital is formally the same as preparation of the pendulum in the upper position. Such a preparation is unstable. If we want to stabilize the pendulum in the upper position we have the following options: (i) introducing periodic driving, which leads to the Kapitza effect; or (ii) introducing noisy driving, which leads to a Zeno effect. We note that the Kapitza effect in the BJJ context has been discussed in Ref. [12], while our interest here is in the semiclassical perspective of the QZE that has been illuminated in Ref. [11].

Experiments with cold atoms are state of the art [13,14]. In such experiments it is common to perform a "fringe visibility" measurement, which indicates the condensate occupation. The latter is commonly quantified in terms of a function $\mathcal{F}(t)$. For the initial coherent preparation $\mathcal{F}(t) = 1$, while later (ignoring quantum recurrences) it decays to a smaller value. Disregarding technical details the *standard* QZE argument

*dcohen@bgu.ac.il

implies an exponential decay,

$$\mathcal{F}(t) = \exp\left\{-\frac{1}{N}\mathcal{S}(t)\right\}, \tag{3}$$

where N is the number of condensed bosons, and

$$\mathcal{S}(t) = \left(\frac{w^2}{D}\right)t. \tag{4}$$

The key realization in Ref. [11] is that $\mathcal{S}(t)$ is in fact the radial spreading in a stochastic process that is described by Eq. (1).

A practical question arises, whether the heuristic QZE expression for $\mathcal{S}(t)$ is *useful* in order to describe the actual decay of the one-body coherence. The answer in Ref. [11] is: (i) The heuristic result is correct only for a very strong noise (small w/D) and holds only during a very short time; and (ii) irrespective of correctness, it is unlikely to obtain a valid estimate of $\mathcal{S}(t)$ in a realistic measurement, because the statistics is lognormal, dominated by far tails.

On the quantitative side, Ref. [11] was unable to provide an analytical theory for the lognormal statistics of the spreading. Rather it has been argued that the $\ln(r)$ distribution has some average $\mu \propto t$ and some variance $\sigma^2 \propto t$. The radial stretching rate w_r and the radial diffusion coefficient D_r were determined *numerically* from the assumed time dependence:

$$\mu = w_r t, \tag{5}$$

$$\sigma^2 = 2D_r t. \tag{6}$$

From the lognormal assumption it follows that

$$\mathcal{S}(t) = e^{4D_r t + 2w_r t} - 1. \tag{7}$$

For strong noise the following asymptotic results have been obtained:

$$w_r \sim \frac{w^2}{4D}, \tag{8}$$

$$D_r \sim \frac{w^2}{8D}. \tag{9}$$

These approximations are satisfactory for $w/D \ll 1$ but fail miserably otherwise. We also see that Eq. (7) reduces to Eq. (4) in this strong-noise limit, for a limited duration of time. Note that Eq. (7) is not identical to the expression that has been reported in Ref. [11], for reasons that are discussed in the concluding section.

The QZE motivation for the analysis of Eq. (1) is introduced in Sec. II. Numerical results for the radial spreading due to this process are presented in Sec. III. Our objective is to find explicit expressions for w_r and D_r and, also, to characterize the full statistics of $r(t)$ in terms of the bare model parameters (w,D). The first step is to analyze the phase randomization in Sec. IV and to discuss the implication of its nonisotropic distribution in Sec. V. Consequently the exact calculation of the $\ln(r)$ diffusion is presented in Secs. VI and VII. In Sec. VIII we clarify that the statistics of $r(t)$ is in fact a *bounded* lognormal distribution. It follows that the r moments of the spreading, unlike the $\ln(r)$ moments, cannot be deduced directly from our results for w_r and D_r. Nevertheless, in Sec. IX we find the r moments using the equation of motion for the moments. Finally, in Sec. X we return to the discussion of the QZE context of our results. On the one hand, we note that Eq. (7) should be replaced by a better version that takes into account the deviations from the lognormal statistics. But the formal result for $\mathcal{S}(t)$ has no experimental significance: The feasibility of experimental $\mathcal{S}(t)$ determination is questionable, because averages are sensitive to the far tails. Rather, in a realistic experiment it is feasible to accumulate statistics and to deduce what are w_r and D_r, which can be tested against our predictions. Some extra details regarding the QZE perspective and other technicalities are provided in the Appendixes.

II. SEMICLASSICAL PERSPECTIVE

In the present section we clarify the semiclassical perspective for the QZE model and motivate the detailed analysis of Eq. (1). The subsequent sections are written in a way that is independent of a specific physical context. We return to the discussion of the QZE in the concluding section, where the implications of our results are summarized.

For a particular realization of $\omega(t)$ the evolution that is generated by Eq. (1) is represented by a symplectic matrix,

$$\begin{pmatrix} x(t) \\ y(t) \end{pmatrix} = \boldsymbol{U}\begin{pmatrix} x_0 \\ y_0 \end{pmatrix}. \tag{10}$$

The matrix is characterized by its trace $a = \text{trace}(\boldsymbol{U})$. If $|a| < 2$, it means an elliptic matrix (rotation). If $|a| > 2$, it means a hyperbolic matrix. In the latter case, the radial coordinate r is stretched in one major direction by some factor $\exp(\alpha)$, while in the other major direction it is squeezed by a factor $\exp(-\alpha)$. Hence $a = \pm 2\cosh(\alpha)$. If we operate with $\boldsymbol{U}$ on an initial isotropic cloud that has radius r_0, then we get a stretched cloud with $\langle r^2\rangle = \mathcal{A}\, r_0^2$, where $\mathcal{A} = \cosh(2\alpha)$. For more details see Appendix A. The numerical procedure of generating a stochastic process that is described by Eq. (1) is explained in Appendix B. Rarely the result is a rotation. So from now on we refer to it as "squeeze."

The initial preparation can be formally described as a minimal wave packet at the origin of phase space. The local canonical coordinates are (x,y), or optionally one can use the polar coordinates (φ,r). The initial spread of the wave packet is $\langle r^2\rangle = \hbar$. In the case of a BJJ the dimensionless Planck constant is related to the number of particles, namely, $\hbar = 2/N$. In the absence of noise ($D = 0$) the wave packet is stretched exponentially in the x direction, which implies a very fast decay of the initial preparation. This decay can be described by the functions $\mathcal{P}(t)$ and $\mathcal{F}(t)$, which give the survival probability of the initial state and the one-body coherence of the evolving state. For precise definitions see Appendix C. Note that $\mathcal{F}(t)$ is defined as the length of the Bloch vector, normalized such that $\mathcal{F}(t) = 1$ for the initial coherent state.

We now consider the implication of having a noisy dephasing term ($D > 0$). The common perspective is to say that this noise acts like a measurement of the r coordinate, which randomizes the phase φ over a time scale $\tau \sim 1/D$, hence introducing a "collapse" of the wave function. The succession of such interventions (see Appendix C) leads to a relatively slow exponential decay of the coherence, namely, $\mathcal{F}(t) = \exp\{-(\hbar/2)\mathcal{S}(t)\}$, where $\mathcal{S}(t)$ is given by Eq. (4). The stronger the noise (D), the slower is the decay of $\mathcal{F}(t)$. A similar observation applies to $\mathcal{P}(t)$. Using a semiclassical perspective [11] it has been realized that

$$\mathcal{S}(t) = \mathcal{A}(t) - \mathcal{A}(0). \tag{11}$$

Note that by definition $\hbar\mathcal{A}(t)$ is the spread $\langle r^2\rangle$ of the evolving phase-space distribution, where $\mathcal{A}(t)$ is normalized such that $\mathcal{A}(0) = 1$.

The well-known QZE expression, Eq. (4), in spite of its popularity, poorly describes the decoherence process [11]. In fact, it agrees with numerical simulations only for extremely short times for which $(w^2/D)t \ll 1$. The semiclassical explanation is as follows: In each τ step of the evolution the phase-space distribution is stretched by a random factor $\lambda_n = \exp[\alpha_n]$, where the α_n are uncorrelated random variables. Hence by the central limit theorem the product $\lambda = \lambda_t \dots \lambda_2\lambda_1$ has a lognormal distribution, where $\log(\lambda)$ has some average $\mu \propto t$ and variance $\sigma^2 \propto t$ that determine an $\mathcal{A}(t)$ and hence an $\mathcal{S}(t)$ that differs from the naive expression of Eq. (4). The essence of the QZE is that μ and σ^2 are inversely proportional to the intensity of the erratic driving. Consequently one has to distinguish three time scales: the "classical" time for phase ergodization $\tau \sim D^{-1}$, which is related to the angular diffusion; the classical time for loss of isotropy $t_r \sim (w^2/D)^{-1}$, which characterizes the radial spreading; and the "quantum" coherence time $t_c \sim (1/\hbar)t_r$, after which $\mathcal{F}(t) \ll 1$.

In Ref. [11] the time dependence of μ and σ has been determined numerically. Here we would like to work out a proper analytical theory. It turns out that a quantitative analysis of the stochastic squeezing process requires going beyond the above heuristic description. The complication arises because what we have is not multiplication of a random number but multiplication of random matrices. Furthermore, we see that the calculation of moments requires going beyond central limit theorem, because they are dominated by the far tails of the distribution.

In the concluding section, Sec. X, we clarify that from an experimental point of view the formal expression $\mathcal{F}(t) = \exp\{-(\hbar/2)\mathcal{S}(t)\}$ is not very useful. For practical purposes it is better to consider the *full* statistics of the Bloch vector and to determine μ and σ via a standard fitting procedure.

III. PRELIMINARY CONSIDERATIONS

Below we do not use a matrix language but address directly the statistical properties of an evolving distribution. In (φ,r) polar coordinates Eq. (1) takes the form

$$\dot{\varphi} = -w\sin(2\varphi) + \omega(t), \tag{12}$$

$$\dot{r} = [w\cos(2\varphi)]r. \tag{13}$$

We see that the equation for the phase decouples, while for the radius

$$\frac{d}{dt}\ln(r(t)) = w\cos(2\varphi). \tag{14}$$

The right-hand side has some finite correlation time $\tau \sim 1/D$, and therefore $\ln(r)$ is like a sum of t/τ uncorrelated random variables. It follows from the central limit theorem that for long times the main body of the $\ln(r)$ distribution can be approximated by a *normal* distribution, with some average $\mu \propto t$ and some variance $\sigma^2 \propto t$. Consequently we can define a radial stretching rate w_r and a radial diffusion coefficient D_r via Eq. (6).

Our objective is to find explicit expressions for w_r and D_r and, also, to characterize the full statistics of $r(t)$ in terms of the bare model parameters (w,D). We see that the statistics of $r(t)$ is described by a *bounded lognormal distribution*.

Some rough estimates are in order. For large D one naively assumes that due to ergodization of the phase $\mu = \langle\cos(2\varphi)\rangle w$ is 0, while $\sigma^2 \sim (w\tau)^2(t/\tau)$. Hence one deduces that $w_r \to 0$, while $D_r \propto w^2/D$. A more careful approach [11] that takes into account the nonisotropic distribution of the phase gives the asymptotic results, Eqs. (8) and (9). The dimensionless parameter that controls the accuracy of this result is w/D. These approximations are satisfactory for $w/D \ll 1$ and fail otherwise (see Figs. 1 and 2). For large w/D we get $w_r \to w$, while $D_r \to 0$.

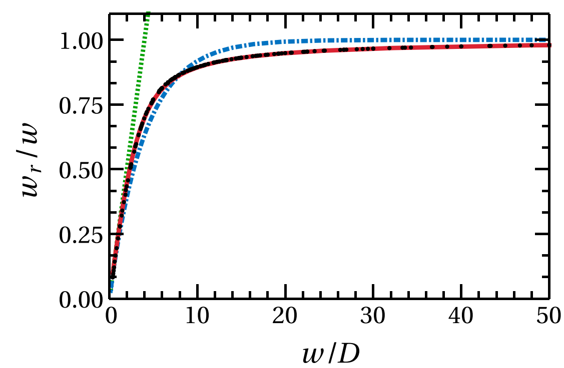

FIG. 1. Scaled stretching rate w_r/w versus w/D. Numerical results (black symbols) are based on simulations with 2000 realizations. Lines represent the naive result, Eq. (8) (dotted green line); the exact result, Eq. (23) (solid red line); and its practical approximation, Eq. (24) (dashed-dotted blue line). For large values of w/D we get $w_r/w = 1$, as for a pure stretch.

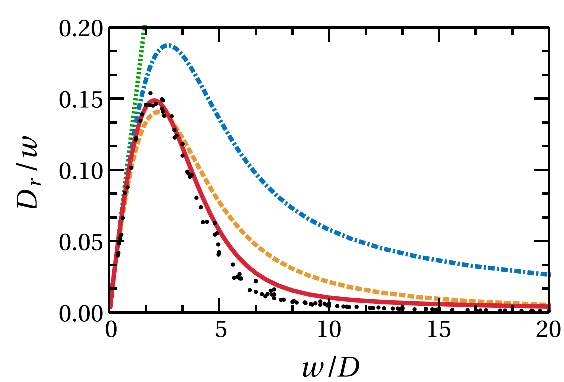

FIG. 2. Scaled diffusion coefficient D_r/w versus w/D. Numerical results (black symbols) are based on simulations with 2000 realizations. Lines represent the naive result, Eq. (9) (dotted green line); the exact result, Eq. (33) (solid red line); and the approximation, Eq. (28), with $\tau = 1/(2D)$ (dashed-dotted blue line) and with Eq. (34) (dashed orange line).

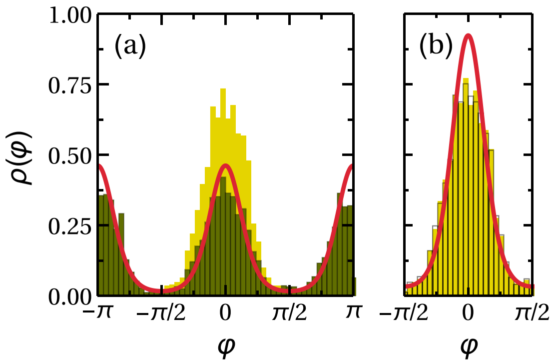

FIG. 3. (a) Phase distribution for $(w/D) = 10/3$ after time $(wt) = 6$, with initial conditions $\varphi = 0$ (yellow region) and $\varphi = \pi/2$ (green bars) and 2000 realizations. For longer times, both reach the steady state of Eq. (16) (red line). (b) Distributions of φ modulo π.

IV. PHASE ERGODIZATION

The Fokker-Planck equation (FPE) that is associated with Eq. (12) is

$$\frac{\partial \rho}{\partial t} = \frac{\partial}{\partial \varphi}\left[\left(D\frac{\partial}{\partial \varphi} + w\sin(2\varphi)\right)\rho\right]. \tag{15}$$

It has the canonical steady-state solution

$$\rho_\infty(\varphi) \propto \exp\left[\frac{w}{2D}\cos(2\varphi)\right]. \tag{16}$$

If we neglect the cosine potential in Eq. (15), then the time for ergodization is $\tau_{\text{erg}} \sim 1/D$. But if w/D is large, we have to incorporate an activation factor; accordingly,

$$\tau_{\text{erg}} = \frac{1}{D}\exp\left[\frac{w}{D}\right]. \tag{17}$$

Figure 3(a) shows the distribution of the phase for two initial conditions, as obtained by a finite-time numerical simulation. It is compared with the steady-state solution. The dynamics of r depends only on 2φ and is dominated by the distribution at the vicinity of $\cos(2\varphi) \sim 1$. We therefore display in Fig. 3(b) the distribution of φ modulo π. We deduce that the transient time of the $\ln(r)$ spreading is much shorter than τ_{erg}.

For the later calculation of w_r we have to know the moments of the angular distribution. From Eq. (16) we obtain

$$X_n \equiv \langle\cos(2n\varphi)\rangle_\infty = \frac{I_n\left(\frac{w}{2D}\right)}{I_0\left(\frac{w}{2D}\right)}. \tag{18}$$

Here $I_n(z)$ are the modified Bessel functions. For small z we have $I_n(z) \approx [1/n!](z/2)^n$, while for large z we have $I_n(z) \approx (2\pi z)^{-1/2}e^z$. The dependence of the X_n on n for representative values of w/D is illustrated in Fig. 4(a).

For the later calculation of D_r we have to know also the temporal correlations. We define

$$C_n(t) = \langle\cos(2n\varphi_t)\cos(2\varphi)\rangle_\infty - X_nX_1, \tag{19}$$

where a constant is subtracted such that $C_n(\infty) = 0$. We use the notations

$$c_n \equiv \int_0^\infty C_n(t)dt \tag{20}$$

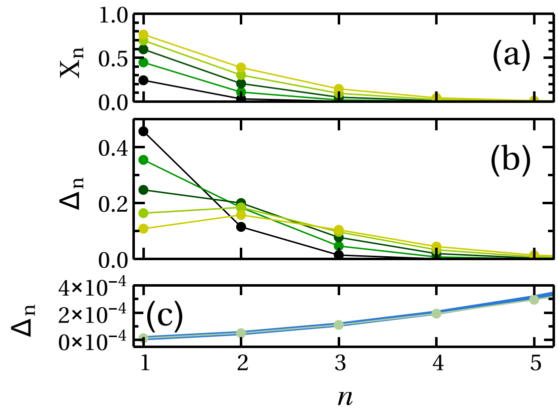

FIG. 4. (a) Values of X_n versus n for some values of w/D. From bottom to top: $w/D = 1, 2, 3, 4, 5$. (b)Values of Δ_n versus n for the same values of w/D, the larger w/D, the smaller Δ_1. (c) Δ_n versus n for large w/D. Here $w/D = 400$. The asymptotic approximation, Eq. (22), is indicated by the blue line.

and

$$\Delta_n \equiv C_n(0) = \tfrac{1}{2}(X_{n+1} + X_{n-1}) - X_nX_1. \tag{21}$$

In order to find an asymptotic expression we use

$$I_n(z) \approx \frac{e^z}{\sqrt{2\pi z}}\left[1 - \frac{4n^2-1}{(8z)} + \frac{(4n^2-1)(4n^2-9)}{2(8z)^2}\right]$$

and get

$$\Delta_n \approx 2\left(\frac{w}{D}\right)^{-2}n^2 \quad \text{for} \quad \left(\frac{w}{D}\right) \gg 1. \tag{22}$$

The dependence of the Δ_n on n for representative values of w/D is illustrated in Figs. 4(b) and 4(c).

V. RADIAL SPREADING

If follows from Eq. (14) that the radial stretching rate is

$$w_r = w\langle\cos(2\varphi)\rangle_\infty = X_1w. \tag{23}$$

A rough interpolation for X_1 that is based on the asymptotic expressions for the Bessel functions in Eq. (18) leads to the following approximation:

$$w_r \approx w\left[1 - \exp\left(-\frac{w}{4D}\right)\right]. \tag{24}$$

The exact result as well as the approximation is illustrated in Fig. 1 and compared with the results of numerical simulations.

For the second moment it follows from Eq. (14) that the radial diffusion coefficient is

$$D_r = w^2\int_0^\infty C_1(t)dt = c_1w^2. \tag{25}$$

If we assume that the ergodic angular distribution is isotropic, the calculation of $C_1(t)$ becomes very simple, namely,

$$C_1(t) = \tfrac{1}{2}\langle\cos 2(\varphi_t - \varphi_0)\rangle = \tfrac{1}{2}e^{-4D|t|}. \tag{26}$$

This expression implies a correlation time $\tau = 1/(2D)$, such that $c_1 = (1/2)\Delta_1\tau$ is half the "area" of the correlation function whose "height" is $\Delta_1 = 1/2$. Thus we get for the radial diffusion coefficient $D_r = w^2/(8D)$.

But in fact the ergodic angular distribution is not isotropic, meaning that X_1 is not 0 and $\Delta_1 < 1/2$. If w is not too large, we may assume that the correlation time τ is not affected. Then it follows that a reasonable approximation for the correlation function is

$$C_1(t) \approx \Delta_1 e^{-2|t|/\tau}, \tag{27}$$

leading to

$$D_r \approx \frac{1}{2}\Delta_1 \tau w^2 = \Delta_1 \frac{w^2}{4D}. \tag{28}$$

This approximation is compared to the exact result that we derive later in Fig. 2. Unlike the rough approximation $D_r = w^2/(8D)$, it captures the observed nonmonotonic dependence of D_r versus w, but quantitatively it is an overestimate.

VI. EXACT CALCULATION OF THE DIFFUSION COEFFICIENT

We now turn to finding an exact expression for the diffusion coefficient, Eq. (25), by calculating c_1 of Eq. (20). Propagating an initial distribution $\rho_0(\varphi)$ with the FPE, Eq. (15), we define the moments:

$$x_n = \langle \cos(2n\,\varphi_t)\rangle_0 = \langle \cos(2n\,\varphi)\rangle_t$$
$$= \int \cos(2n\,\varphi)\rho_t(\varphi)d\varphi. \tag{29}$$

The moments equation of motion resulting from the FPE is [15]

$$\frac{d}{dt}x_n = -\Lambda_n\, x_n + W_n(x_{n-1} - x_{n+1}), \tag{30}$$

where $\Lambda_n = 4Dn^2$ and $W_n = wn$. Due to $\Lambda_0 = W_0 = 0$ the zeroth moment $x_0 = 1$ does not change in time. Thus the rank of Eq. (30) is less than its dimension reflecting the existence of a zero mode $x_n = X_n$ that corresponds to the steady state of the FPE. We use the subscript "∞" to indicate the steady-state distribution. Any other solution $x_n(t)$ goes to X_n in the long-time limit, while all the other modes are decaying. To find X_n the equation should be solved with the boundary condition $X_\infty = 0$ and normalized such that $X_0 = 1$. Clearly this is not required in practice: because we already know the steady-state solution, Eq. (15), hence Eq. (18).

We define $x_n(t;\varphi_0)$ as the time-dependent solution for an initial preparation $\rho_0(\varphi) = \delta(\varphi - \varphi_0)$. Then we can express the correlation function of Eq. (19) as follows:

$$C_n(t) = \langle x_n(t;\varphi)\cos(2\varphi)\rangle_\infty - X_n X_1. \tag{31}$$

By linearity the $C_n(t)$ obey the same equation of motion as do the $x_n(t)$, but with the special initial conditions $C_n(0) = \Delta_n$. Note that $C_0(t) = 0$ at any time. In the infinite-time limit $C_n(\infty) = 0$ for any n.

Our interest is in the area c_n as defined in Eq. (20). Writing Eq. (30) for $C_n(t)$ and integrating it over time we get

$$\Lambda_n\, c_n - W_n(c_{n-1} - c_{n+1}) = \Delta_n. \tag{32}$$

This equation should be solved with the boundary conditions $c_0 = 0$ and $c_\infty = 0$. The solution is unique because the $n = 0$ site has been effectively removed, and the truncated matrix is no longer with zero mode. One possible numerical procedure is to start iterating with c_1 as initial condition and to adjust it such that the solution will go to 0 at ∞. An optional procedure is to integrate the recursion backwards as explained in the next section. The bottom line is the expression

$$D_r = c_1 w^2 = -\sum_{n=1}^{\infty}\frac{(-1)^n}{n}\Delta_n X_n w, \tag{33}$$

where X_n and Δ_n are given by Eq. (18) and Eq. (21), respectively.

The leading term approximation $D_r \approx \Delta_1 X_1 w$ is consistent with the heuristic expression $D_r \approx (1/2)\Delta_1 \tau w^2$ of Eq. (28) upon the identification

$$\tau = \frac{2}{w}\left[1 - \exp\left(-\frac{w}{4D}\right)\right]. \tag{34}$$

This expression reflects the crossover from diffusion-limited ($\tau \propto 1/D$) to drift-limited ($\tau \propto 1/w$) spreading. Figure 2 compares the approximation that is based on Eq. (28) with Eq. (34) to the exact result, Eq. (33).

In the limit $(w/D) \to 0$ the asymptotic result for the radial diffusion coefficient is $D_r = w^2/(8D)$. We now turn to figing out the asymptotic result in the other extreme limit $(w/D) \to \infty$. The large-w/D approximation, which is based on the first term of Eq. (33), with the limiting value $X_1 = 1$, provides the asymptotic estimate $D_r \approx 2D^2/w$. This expression is based on the asymptotic result, Eq. (22), for Δ_n with $n = 1$. In fact we can do better and add all the higher order terms. Using Abel summation we get

$$D_r = 2\frac{D^2}{w}\sum_{n=1}^{\infty}(-1)^{n-1}n = \frac{1}{2}\frac{D^2}{w}. \tag{35}$$

Thus the higher order terms merely add a factor 1/4 to the asymptotic result. If we used Eq. (28), we would have obtained the wrong prediction $D_r \approx D/2$, which ignores the τ dependence of Eq. (34).

VII. DERIVATION OF THE RECURSIVE SOLUTION

In this section we provide the details of the derivation that leads from Eq. (32) to Eq. (33). We define $W_n^{\pm} = \mp W_n$ and rewrite the equation in the more general form

$$-W_n^+ c_{n+1} + \Lambda_n c_n - W_n^- c_{n-1} = \Delta_n. \tag{36}$$

A similar problem was solved in Ref. [16], while here we present a much simpler treatment. First, we solve the associated homogeneous equation. The solution $c_n = X_n$ satisfies

$$-W_n^+ X_{n+1} + \Lambda_n X_n - W_n^- X_{n-1} = 0 \tag{37}$$

and one can define the ratios $R_n = X_n/X_{n-1}$. Note that these ratios satisfy a simple first-order recursive relation. However, we bypass this stage because we can extract the solution from the steady-state distribution.

We write the solution of the nonhomogeneous equation as

$$c_n := X_n \tilde{c}_n \tag{38}$$

and we get the equation

$$-W_n^+ X_{n+1}\tilde{c}_{n+1} + \Lambda_n X_n \tilde{c}_n - W_n^- X_{n-1}\tilde{c}_{n-1} = \Delta_n.$$

Clearly it can be rewritten as

$$-W_n^+ X_{n+1}(\tilde{c}_{n+1} - \tilde{c}_n) + W_n^- X_{n-1}(\tilde{c}_n - \tilde{c}_{n-1}) = \Delta_n.$$

We define the discrete derivative

$$\tilde{a}_n := \tilde{c}_n - \tilde{c}_{n-1} \tag{39}$$

and obtain a reduction to a first-order equation:

$$-W_n^+ X_{n+1}\tilde{a}_{n+1} + W_n^- X_{n-1}\tilde{a}_n = \Delta_n. \tag{40}$$

This can be rewritten in a simpler way by appropriate definition of scaled variables. Namely, we define the notations

$$\tilde{R}_n = \frac{W_n^+}{W_n^-} R_n, \quad \tilde{\Delta}_n = \frac{\Delta_n}{W_n^+} \tag{41}$$

and the rescaled variable

$$a_n := X_n \tilde{a}_n \tag{42}$$

and then solve the a_n recursion in the backwards direction:

$$a_\infty = 0, \quad a_n = \tilde{R}_n[\tilde{\Delta}_n + a_{n+1}]. \tag{43}$$

If all the R_n were unity, it would imply that $a_1 - a_\infty$ equals $\sum \Delta_n$. So it is important to verify that the "area" converges. Next we can solve in the forward direction the c_n recursion for the nonhomogeneous equation, namely,

$$c_0 = 0, \quad c_n = R_n c_{n-1} + a_n. \tag{44}$$

In fact we are only interested in

$$c_1 = a_1 = \tilde{R}_1\tilde{\Delta}_1 + \tilde{R}_1\tilde{R}_2\tilde{\Delta}_2 + \cdots. \tag{45}$$

Note that in our calculation $\tilde{R}_n = -R_n$, and therefore $\tilde{R}_1 \ldots \tilde{R}_n = (-1)^n X_n$.

VIII. MOMENTS OF THE RADIAL SPREADING

The moments of a lognormal distribution are given by the following expression:

$$\ln\langle r^n\rangle = \mu n + \tfrac{1}{2}\sigma^2 n^2. \tag{46}$$

On the basis of the discussion following Eq. (14), if one assumed that the radial spreading at time t could be *globally* approximated by the lognormal distribution (tails included), it would follow that

$$\frac{d}{dt}\ln\langle r^n\rangle = n w_r + n^2 D_r. \tag{47}$$

In Fig. 5 we plot the lognormal-based expected growth rate of the second and the fourth moments as a function of w/D. For small w/D there is good agreement with the expected results, which are w^2/D and $3w^2/D$, respectively. For large w/D the dynamics is dominated by the stretching, meaning that $w_r \approx w$, while $D_r \to 0$, so again we have a trivial agreement. But for intermediate values of w/D the lognormal moments constitute an overestimate compared with the exact analytical results that we derive in the next section. In fact also the exact analytical result looks like an overestimate compared with the results of numerical simulations. But the latter is clearly a sampling issue that is explained in Appendix D.

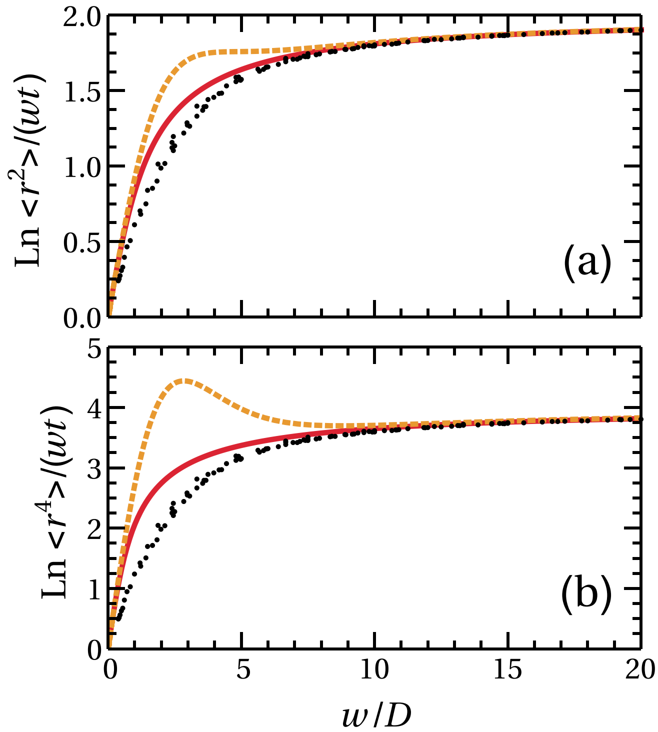

FIG. 5. Scaled moments versus w/D. Solid red lines are the exact results for the second and fourth moments, given by Eq. (48) and Eq. (60), and the large w/D asymptotic values are at 2 and 4, respectively. These are compared with the numerical results (black symbols) and contrasted with the lognormal prediction (dashed orange lines). The latter provides an overestimate for intermediate values of w/D.

The deviation of the lognormal moments from the exact results indicates that the statistics of large deviations is not captured by the central limit theorem. This point is illustrated in Fig. 6. The Gaussian approximation constitutes a good approximation for the body of the distribution but not for

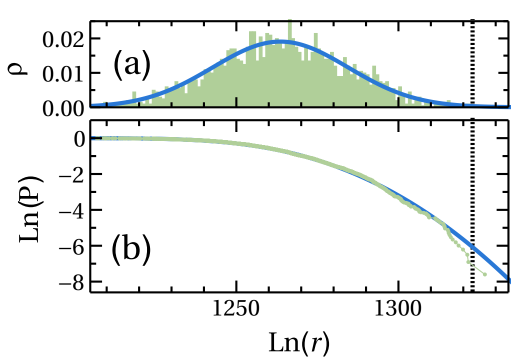

FIG. 6. (a) Distribution of $\ln(r)$ for $w/D = 10/3$ after time $wt = 2000$ with initial conditions $r = 1$ and $\varphi = 0$. Numerical results (green histogram), which are based on 2000 realizations, are fitted to a Gaussian distribution (blue line). (b) Inverse cumulative probability of the same distribution. The dotted black line indicates the numerically determined value $\ln\langle r^2\rangle^{1/2} \approx 1323$. This value is predominated by the tail of the distribution. The Gaussian fit fails to reproduce this value and provides a gross overestimate, $\ln\langle r^2\rangle^{1/2} \approx 1701$.

the tails that dominate the moment calculation. Clearly, the actual distribution can be described as a *bounded* lognormal distribution, meaning that it has a natural cutoff which is implied by the strict inequality $w_r < w$. The stretching rate cannot be faster than w. But in fact, as shown in Fig. 6(b), the deviation from the lognormal distribution occurs even before the cutoff is reached.

Below we carry out an exact calculation for the second and fourth moments. In the former case we show that

$$\frac{d}{dt}\ln\langle r^2\rangle \sim 2((w^2+D^2)^{1/2}-D). \tag{48}$$

This agrees with the lognormal-based prediction w^2/D for $(w/D) \ll 1$ and goes to $2w$ for $(w/D) \gg 1$, as could be anticipated.

Before we consider the derivation of this result we would like to illuminate its main features by considering a simple reasoning. Let us ask ourselves what the result would be if the spreading were isotropic ($w_r = 0$). In this case the moments of spreading can be calculated as if we are dealing with the multiplication of random numbers. Namely, assuming that the duration of each step is $\tau = 1/(2D)$ and treating t as a discrete index, Eq. (13) implies that the spreading is obtained by multiplication of uncorrelated stretching factors $\exp[w\tau\cos(\varphi)]$. Each stretching exponent has zero mean and dispersion $\sigma_1^2 = (1/2)[w\tau]^2$, which implies $D_r = \sigma_1^2/(2\tau)$. Consequently we get for the moments

$$\langle r^n\rangle = [\langle e^{nw\tau\cos(2\varphi)}\rangle]^{t/\tau} r_0^n, \tag{49}$$

leading to

$$\frac{d}{dt}\ln\langle r^n\rangle = \frac{1}{\tau}\ln[I_0(\sqrt{2}n\sigma_1)]. \tag{50}$$

This gives a crossover from n^2D_r for $\sigma_1 \ll 1$ to nw for $\sigma_1 \gg 1$, reflecting isotropic lognormal spreading in the former case and pure stretching in the latter case. So again we see that the asymptotic limits are easily understood, but for the derivation of the correct interpolation, say Eq. (48), further effort is required.

IX. EXACT CALCULATION OF THE MOMENTS

We here perform an exact calculation of the moments. One can associate with the Langevin equation, Eq. (1), an FPE for the distribution and, from that, derive the equation of motion for the moments. The procedure is explained and summarized in Appendix E. For the first moments we get

$$\frac{d}{dt}\langle x\rangle = w\langle x\rangle - D\langle x\rangle, \tag{51}$$

$$\frac{d}{dt}\langle y\rangle = -w\langle y\rangle - D\langle y\rangle, \tag{52}$$

with the solution

$$\langle x\rangle = x_0\exp[-(D-w)t], \tag{53}$$

$$\langle y\rangle = y_0\exp[-(D+w)t]. \tag{54}$$

For the second moments

$$\frac{d}{dt}\begin{pmatrix}\langle x^2\rangle\\ \langle y^2\rangle\end{pmatrix} = [-2D + 2D\boldsymbol{\sigma}_1 + 2w\boldsymbol{\sigma}_3]\begin{pmatrix}\langle x^2\rangle\\ \langle y^2\rangle\end{pmatrix}, \tag{55}$$

$$\frac{d}{dt}\langle xy\rangle = -4D\langle xy\rangle, \tag{56}$$

where $\boldsymbol{\sigma}$ are Pauli matrices. The solution is

$$\begin{pmatrix}\langle x^2\rangle\\ \langle y^2\rangle\\ \langle xy\rangle\end{pmatrix} = \begin{bmatrix} e^{-2Dt}\boldsymbol{M} & 0\\ 0 & e^{-4Dt}\end{bmatrix}\begin{pmatrix}x_0^2\\ y_0^2\\ x_0y_0\end{pmatrix}, \tag{57}$$

where $\boldsymbol{M}$ is the following matrix:

$$\cosh[2(w^2+D^2)^{1/2}t] + \sinh[2(w^2+D^2)^{1/2}t]\frac{D\boldsymbol{\sigma}_1 + w\boldsymbol{\sigma}_3}{\sqrt{w^2+D^2}}.$$

For an initial isotropic distribution we get $\langle r^2\rangle_t = Mr_0^2$, where

$$M = e^{-2Dt}\cosh[2(w^2+D^2)^{1/2}t] + \frac{D}{\sqrt{w^2+D^2}}e^{-2Dt}\sinh[2(w^2+D^2)^{1/2}t]. \tag{58}$$

The short-time t dependence is quadratic, reflecting "ballistic" spreading, while for long times

$$\langle r^2\rangle_t \approx \frac{r_0^2}{2}\left(1+\frac{D}{\sqrt{w^2+D^2}}\right) \times \exp[2((w^2+D^2)^{1/2}-D)t]. \tag{59}$$

From here we get Eq. (48). For the fourth moments the equations are separated into two blocks of even-even powers and odd-odd powers in x and y. For the even block,

$$\frac{d}{dt}\begin{pmatrix}\langle x^4\rangle\\ \langle x^2y^2\rangle\\ \langle y^4\rangle\end{pmatrix} = 2\tilde{\boldsymbol{M}}\begin{pmatrix}\langle x^4\rangle\\ \langle x^2y^2\rangle\\ \langle y^4\rangle\end{pmatrix}, \tag{60}$$

where

$$\tilde{\boldsymbol{M}} = \begin{pmatrix} 2(w-D) & 6D & 0\\ D & -6D & D\\ 0 & 6D & -2(w+D)\end{pmatrix}. \tag{61}$$

The eigenvalues of this matrix are the solution of $\lambda^3 + 10D\lambda^2 + (16D^2 - 4w^2)\lambda - 24Dw^2 = 0$. There are two negative roots and one positive root. For small w/D the latter is $\lambda \approx (3/2)(w^2/D)$, and we get that the growth rate is $3w^2/D$ as expected from the log-normal statistics.

X. DISCUSSION

In this work we have studied the statistics of a stochastic squeeze process, defined by Eq. (1). Consequently we are able to provide a quantitatively valid theory for the description of the noise-affected decoherence process in bimodal Bose-Einstein condensates, a.k.a. the QZE. As the ratio w/D is increased, the radial diffusion coefficient of $\ln(r)$ changes in a nonmonotonic way from $D_r = w^2/(8D)$ to $D_r = D^2/(2w)$, and the nonisotropy is enhanced, namely, the average stretching rate increases from $w_r = w^2/(4D)$ to the bare value $w_r = w$. The analytical results, Eq. (23) and Eq. (33), are illustrated in Fig. 1 and Fig. 2,

Additionally we have solved for the moments of r. One observes that the central limit theorem is not enough for this calculation, because the moments are predominated by the non-Gaussian tails of the $\ln(r)$ distribution. In particular, we have derived for the second moment the expression $\langle r^2\rangle_t = M r_0^2$, with M given by Eq. (58), or optionally one can use the practical approximation, Eq. (48).

The main motivation for our work comes form the interest in the BJJ. From the mathematical point of view the BJJ can be regarded as a quantum pendulum. It has both stable and unstable fixed points. Its dynamics has been explored by numerous experiments. We mention, for example, Ref. [17], in which both Josephson oscillations ("liberations") and self-trapping ("rotations") were observed, and Ref. [18], in which a.c. and d.c. Josephson effects were observed. The phase space of the device is spherical, known as the Bloch sphere. A quantum state corresponds to a quasidistribution (Wigner function) on that sphere and can be characterized by the Bloch vector $\vec{S}$. The length $\mathcal{F} = |\vec{S}|$ of the Bloch vector reflects the one-body coherence and has to do with the "fringe visibility" in a time-of-flight measurement. If all the particles are initially condensed in the upper orbital of the BJJ, it corresponds to a coherent $\mathcal{F} = 1$ wave packet that is positioned on top of the hyperbolic point, which corresponds to the upper position of the pendulum. The dynamics has been thoroughly analyzed in Ref. [2] and experimentally demonstrated in Ref. [3].

To the best of our knowledge, neither the Kapitza effect [12] nor the Zeno effect has been demonstrated experimentally in the BJJ context. We expect the decay of $\mathcal{F}$ to be suppressed due to the periodic or the noisy driving, respectively. Let us clarify the experimental significance of our results for the full statistics of the radial spreading in the latter case. In order to simplify the discussion, let us assume that the definition of $\mathcal{F}$ is associated with the measurement of a single coordinate $\hat{x}$. Measurement of $\hat{x}$ is essentially the same as probing of an occupation difference. From the semiclassical perspective (Wigner function picture) the phase-space coordinate x satisfies Eq. (1), where $\omega(t)$ arises from frequent interventions, or measurements, or noise that comes from the surroundings. Using the Feynman-Vernon perspective, each x outcome of the experiment can be regarded as the result of one realization of the stochastic process. The "coherence" is determined by the second moment of $\hat{x}$. But it is implied by our discussion of the *sampling problem* that it is impractical to determine this second moment from any realistic experiment (rare events are not properly accounted). The reliable experimental procedure would be to keep the *full* probability distribution of the measured x variable and to extract the μ and the σ that characterize its lognormal statistics. For the latter we predict nontrivial dependence on w/D.

Still, from a purely mathematical point of view, one might be curious about the validity of the heuristic QZE expression, Eq. (4). We have pointed out in Sec. I that the lognormal assumption implies that it should be replaced by Eq. (7), which reduces to Eq. (4) only for short times if the noise is very strong (small w/D). We note that the expression reported originally in Ref. [11] was slightly different, namely,

$$\mathcal{S}(t) = e^{4D_r t}\cosh(2w_r t) - 1. \tag{62}$$

The difference is due to the assumption (there) that it is α, as defined in Appendix A, rather than r, which has a lognormal distribution. In physical terms this is like ignoring the initial isotropy of the preparation, hence creating an artifact—an artificial transient. In any case we found in the present work that none of these expressions are correct. This is because the tail of the distribution is bounded. From Eq. (48) we deduce that a practical approximation would be

$$\mathcal{S}(t) = 2((w^2 + D^2)^{1/2} - D)\,t. \tag{63}$$

Note that both Eq. (7) and Eq. (63) agree with the heuristic expectation $(w^2/D)t$ for $(w/D) \ll 1$ and goes to the bare nonsuppressed value $2wt$ for $(w/D) \gg 1$. The difference between them is at intermediate values of w/D, where the lognormal prediction is an overestimate. On the other hand, in a realistic experiment, we expect an underestimate as illustrated in Fig. 5.

APPENDIX A: THE SQUEEZE OPERATION

The squeeze operation is described by a real symplectic matrix that has unit determinant and trace $|a| > 2$. Any such matrix can be expressed as

$$\boldsymbol{U} = \begin{pmatrix} a & b \\ c & d \end{pmatrix} = \pm e^{\alpha \boldsymbol{H}} \quad [ad - cb = 1], \tag{A1}$$

where $\mathbf{H}$ is a real traceless matrix that satisfies $\boldsymbol{H}^2 = 1$. Hence it can be expressed as a linear combination of the three Pauli matrices,

$$\boldsymbol{H} = n_1\boldsymbol{\sigma}_1 + i n_2\boldsymbol{\sigma}_2 + n_3\boldsymbol{\sigma}_3, \tag{A2}$$

with $n_1^2 - n_2^2 + n_3^2 = 1$. Consequently,

$$\boldsymbol{U} = \pm[\cosh(\alpha)\mathbf{1} + \sinh(\alpha)\boldsymbol{H}]. \tag{A3}$$

We define the canonical form of the squeeze operation as

$$\boldsymbol{\Lambda} = \begin{pmatrix} \exp(\alpha) & 0 \\ 0 & \exp(-\alpha) \end{pmatrix}. \tag{A4}$$

Then we can obtain any general squeeze operation via similarity transformation, which involves rescaling of the axes and rotation and, on top, an optional reflection.

We can operate with $\boldsymbol{U}$ on an initial isotropic cloud that has radius $r_0 = 1$. Then we get a stretched cloud that has spread $\langle r^2\rangle = \mathcal{A} r_0^2$, where

$$\mathcal{A} \equiv \langle r^2\rangle|_{r_0=1} = \cosh(2\alpha). \tag{A5}$$

We also define the "spreading" as

$$\mathcal{S} = \mathcal{A} - 1 = 2\sinh^2(\alpha). \tag{A6}$$

The notation α has no meaning for a *stochastic* squeeze process, while the notation $\mathcal{A} \equiv \langle r^2\rangle$ can still be used. In the latter case the average is over the initial conditions and also over realizations of $\omega(t)$, implying that in Eq. (A5) the $\cosh(2\alpha)$ should be averaged over α.

APPENDIX B: NUMERICAL SIMULATIONS

There are numerous numerical schemes that allow the simulation of a Langevin equation, for example, the Milstein, the Runge-Kutta, and higher-order approximations such as the truncated Taylor expansion [19]. These schemes are based on iterative integration of the Langevin equation, then Taylor expansion of the solution in small dt. The dynamics generated by Eq. (1) is symplectic, however, the numerical methods listed above do not respect this constraint. Instead one can exploit the linear nature of the problem. Namely, Eq. (1) is rewritten as

$$\dot{\boldsymbol{r}}_t = \boldsymbol{H}(t)\boldsymbol{r}_t, \tag{B1}$$

$$\boldsymbol{H} = \boldsymbol{H}_s + \boldsymbol{H}_r(t), \tag{B2}$$

where $\boldsymbol{H}_s$ and $\boldsymbol{H}_r$ are the generators of the stretching and the angular diffusion, respectively, while $\boldsymbol{r}_t = (x_t, y_t)$. If $\boldsymbol{H}_r$ were constant, the solution of Eq. (B1) would be obtained by simple exponentiation of $\boldsymbol{H}$, namely, $\boldsymbol{r}_{t_f} = \boldsymbol{U}\boldsymbol{r}_0$, with $\boldsymbol{U} = \exp[(\boldsymbol{H}_r + \boldsymbol{H}_s)t_f]$. Choosing a small enough time interval dt and using the Suzuki-Trotter formula, the latter equation is approximated by

$$\boldsymbol{U} = \boldsymbol{U}_{t_f} \dots \boldsymbol{U}_{3dt}\boldsymbol{U}_{2dt}\boldsymbol{U}_{dt}, \tag{B3}$$

$$\boldsymbol{U}_t = \exp(\boldsymbol{H}_s dt)\exp(\boldsymbol{H}_r dt), \tag{B4}$$

where $\boldsymbol{U}_t$ gives the evolution of the vector $\boldsymbol{r}_t$ for short-time dt, namely, $\boldsymbol{r}_t = \boldsymbol{U}_t\boldsymbol{r}_{t-dt}$. Equation (B3) is valid also for time-dependent $\boldsymbol{H}$, where the small step evolution, Eq. (B4), takes the form

$$\boldsymbol{U}_t = \begin{pmatrix} e^{w\,dt} & 0 \\ 0 & e^{-w\,dt} \end{pmatrix}\begin{pmatrix} \cos\alpha_t & -\sin\alpha_t \\ \sin\alpha_t & \cos\alpha_t \end{pmatrix}. \tag{B5}$$

The uncorrelated random variables α_t have zero mean and are taken from a box distribution of width $\sqrt{24D\,dt}$, such that their variance is $2D\,dt$. As a side note we remark that with Taylor expansion of Eq. (B5) to second order in dt, the Milstein scheme is recovered. The radial coordinate r is calculated under the assumption that the preparation is $(x_0 = 1,\ y_0 = 0)$. Accordingly, what we calculate for each realization is

$$r = \sqrt{U_{xx}^2 + U_{yx}^2}. \tag{B6}$$

In Fig. 7(a) we display the distribution of trace a for many realizations of this stochastic squeeze process. Rarely the result is a rotation, and therefore in the text we refer to it as "squeeze." From the trace we get the squeeze exponent α, and from Eq. (B6) we get the radial coordinate r. The correlation between these two squeeze measures is illustrated in Fig. 7(b). For the long-time simulations that we perform in order to extract various moments, we observe full correlation (not shown). In order to extract the various moments, we perform the simulation for a maximum time of $wt = 7500$, with the initial condition $\boldsymbol{r}_0 = (1,0)$.

We note that the results in Sec. IX for the evolution of the moments can be recovered by averaging over the product of the evolution matrices. For the first moments we get the linear relation $\langle \boldsymbol{r}_t\rangle = \langle \boldsymbol{U}\rangle \boldsymbol{r}_0$, where

$$\begin{aligned}\langle \boldsymbol{U}\rangle &= \langle \dots \boldsymbol{U}_{t_3}\boldsymbol{U}_{t_2}\boldsymbol{U}_{t_1}\rangle = [\langle \boldsymbol{U}_t\rangle]^{t/dt} \\ &= \begin{pmatrix} e^{-(D+w)t} & 0 \\ 0 & e^{-(D-w)t} \end{pmatrix}.\end{aligned} \tag{B7}$$

A similar procedure can be applied for calculation of the higher moments.

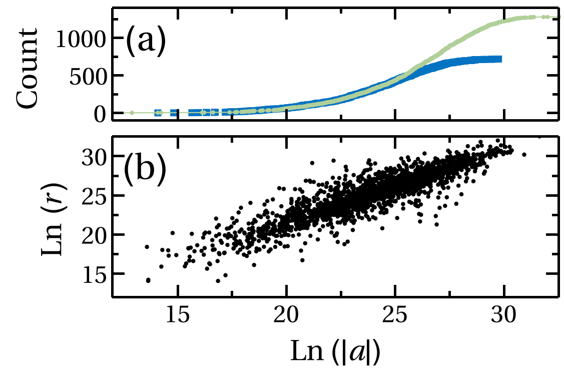

FIG. 7. We consider 2000 realizations of a stochastic squeeze process. For each realization trace $a = \text{trace}(\boldsymbol{U})$ is calculated. (a) Cumulative count of the a values. Green circles represent positive values; blue rectangle, negative values. Here $(w/D) = 10/3$ and $wt = 40$. For simulations with longer times the distributions of positive and negative values become identical (not shown). (b) Scatterplots of $|a|$ versus the radial coordinate r. For simulations with longer times we get a full correlation.

APPENDIX C: RELATION TO THE QZE

It is common to represent the quantum state of the bosonic Josephson junction by a Wigner function on the Bloch sphere (see [2] for details). A coherent state is represented by a Gaussian-like distribution, namely,

$$\rho^{(0)}(x,y) \approx 2\exp\left[-\frac{1}{\hbar}(x^2+y^2)\right], \tag{C1}$$

where x and y are local conjugate coordinates. The Wigner function is properly normalized with the integration measure $dxdy/(2\pi\hbar)$. The dimensionless Plank constant is related to the number N of bosons, namely, $\hbar = (N/2)^{-1}$. After a squeeze operation one obtains a new state, $\rho^{(t)}(x,y)$. The survival probability is

$$\mathcal{P}(t) = \mathrm{Tr}\,[\rho^{(0)}\rho^{(t)}] = \frac{1}{\cosh(\alpha)} = \frac{1}{1+\frac{1}{2}\mathcal{S}(t)}. \tag{C2}$$

However, it is more common, both theoretically and experimentally, to quantify the decay of the initial state via the length of the Bloch vector, namely, $\mathcal{F}(t) = |\vec{S}(t)|$. It has been explained in Ref. [11] that

$$\mathcal{F}(t) \approx \exp\{-\hbar\sinh^2(\alpha)\} = \exp\left\{-\frac{\hbar}{2}\mathcal{S}(t)\right\}. \tag{C3}$$

Compared with the short-time approximation of Eq. (C2), namely, $\mathcal{P} \approx \exp[-(1/2)\mathcal{S}(t)]$, note the additional $\hbar = 2/N$ factor in Eq. (C3). This should be expected: the survival probability drops to 0 even if a single particle leaves the condensate. Contrary to that, the fringe visibility reflects the expectation value of the condensate occupation, and hence its decay is much slower. Still, both depend on the spreading $\mathcal{S}(t)$.

The dynamics that is generated by Eq. (1) does not change the direction of the Bloch vector but, rather, shortens its length, meaning that the one-body coherence is diminished, reflecting the decay of the initial preparation. Using the same coordinates as in Ref. [11] the Bloch vector is $\vec{S}(t) = (S,0,0)$, hence all the information is contained in the measurement of a single observable, a.k.a. the fringe visibility measurement.

For a noiseless canonical squeeze operation we have $D = 0$ and $\alpha = wt$, hence one obtains $\mathcal{S}(t) = 2\sinh^2(wt)$, which is quadratic for short times. In contrast to that, for a stochastic squeeze process Eq. (C3) should be averaged over realizations of $\omega(t)$. Thus $\mathcal{F}(t)$ is determined by the full statistics that we have studied in this paper.

At this point we would like to remind the reader of the common QZE argument that leads to the estimate of Eq. (4). One assumes that for strong D the time for phase randomization is $\tau = 1/(2D)$. Dividing the evolution into τ steps and assuming that at the end of each step the phase is totally randomized (as in projective measurement), one obtains

$$\overline{\mathcal{A}(t)} \approx [\overline{\mathcal{A}(\tau)}]^{t/\tau} \approx [1 - 2(w\tau)^2]^{t/\tau} \tag{C4}$$

$$\approx \exp[-(w^2/D)t]. \tag{C5}$$

The overbar indicates the average over realizations, as discussed following Eq. (A5). The short-time expansion of the exponent is linear rather than quadratic, and the standard QZE expression, Eq. (4), is recovered. This approximation is justified in the "Fermi golden rule regime," namely, for $\tau \ll t \ll t_r$, during which the deviation from isotropy can be treated as a first-order perturbation. For longer times, and definitely for weaker noise, the standard QZE approximation cannot be trusted.

APPENDIX D: SAMPLE MOMENTS OF A LOGNORMAL DISTRIBUTION

Consider a lognormal distribution of r values. This mean that the $\ln r$ values have a Gaussian distribution. For a finite sample of N values, one can calculate the sample average and the sample variance of the $\ln r$ values in order to get a *reliable* estimate for μ and σ and then calculate the moments $\langle r^n\rangle$ via Eq. (46). But a direct calculation of these moments provides a gross underestimate as illustrated in Fig. 8. This is because

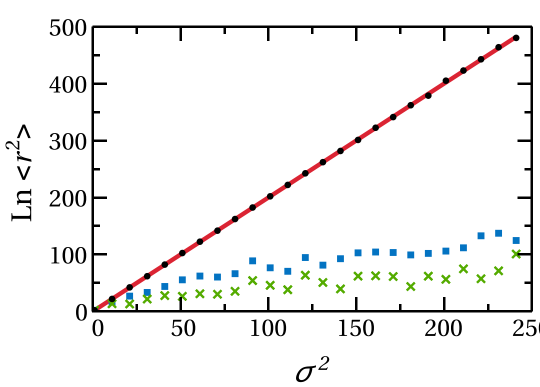

FIG. 8. $\ln\langle r^2\rangle$ versus σ for a lognormal distribution. Without loss of generality $\mu = 0$. The true result is represented by the red line. Numerical estimates based on 10^2 and 10^5 realizations are indicated by green crosses and blue rectangles, respectively. For the latter set of realizations we get a much better estimate using an optional procedure (black circles). Namely, we calculate the sample average and the sample variance of the $\ln r$ values in order to determine μ and σ and then use Eq. (46) to estimate the moments.

the direct average is predominated by rare values that belong to the tail of the distribution.

The lesson is that direct calculation of moments for a logwide distribution cannot be trusted. It can provide a lower bound to the true results, not an actual estimate.

APPENDIX E: FOKKER-PLANCK EQUATION FROM A LANGEVIN EQUATION

We provide a short derivation for the FPE that is associated with a given Langevin equation. From this we obtain the equations of motion for observables. For the sake of generality we write the Langevin equation as follows:

$$\dot{x_j} = v_j + g_j\,\omega(t) \equiv f_j, \tag{E1}$$

$$\langle\omega(t)\omega(t')\rangle = 2D\delta_\tau(t-t'). \tag{E2}$$

The v_j and the g_j are some functions of the x_i. Equation (1) is obtained upon the identification $x_j = (x,y)$ and $v_j = (wx,-wy)$, and $g_j = (-y,x)$. The "noise" has zero average, namely, $\langle\omega(t)\rangle = 0$, and is characterized by a correlation time τ. Accordingly $\delta_\tau(t-t')$ has a short but finite width, which is later taken to be 0.

For a particular realization of the noise, the continuity equation for the Liouville distribution $\rho(x)$ reads

$$\frac{\partial\rho}{\partial t} = -\frac{\partial}{\partial x_j}(f_j\rho). \tag{E3}$$

We are interested in $\rho(x)$ averaged over many realizations of the noise ω. In its current form Eq. (E3) cannot be averaged, because ρ and f are not independent variables. To overcome this issue Eq. (E3) is integrated iteratively. To second order one obtains

$$\rho(t+dt) - \rho(t) = -\int_t^{t+dt} dt' \frac{\partial}{\partial x_j} f_j(t') \times \left[\rho(t) - \int_t^{t'} dt'' \frac{\partial}{\partial x_k} f_k(t'')\rho(t)\right]. \tag{E4}$$

Performing the average over realizations of the noise, a nonvanishing noise-related term arises from the correlator of Eq. (E2). Then performing the dt'' integral over the broadened δ one obtains a 1/2 factor. Dividing both sides by dt and taking the limit $dt \to \tau \to 0$, one obtains

$$\frac{\partial\rho}{\partial t} = -\frac{\partial}{\partial x_j}\left[v_j\rho - g_j D\frac{\partial}{\partial x_i}(g_i\rho)\right]. \tag{E5}$$

Terms that originate from higher order iterations or moments are $\mathcal{O}(dt)$ or vanish in the $\tau \to 0$ limit. Equation (E5) is the FPE that is associated with the Stratonovich interpretation of Eq. (E1) (see Eq. (4.3.45) on p. 100 of [20]).

An observable X is a function of the x variables. In order to obtain an equation of motion for $\langle x\rangle$, we multiply both sides of Eq. (E5) by X and integrate over x. Using integration by parts and dropping the boundary terms, we get the desired equation:

$$\frac{d}{dt}\langle x\rangle = \left\langle\frac{\partial X}{\partial x_j}\left(v_j + \frac{\partial g_j}{\partial x_i}Dg_i\right)\right\rangle + \left\langle\frac{\partial^2 X}{\partial x_i\partial x_j}g_j D g_i\right\rangle. \tag{E6}$$

In the text we use this equation for the moments of the distribution $(x, y, x^2, xy, y^2, x^4, x^2y^2, y^4)$.

Remark concerning various interpretations of the Langevin equation: The Langevin equation defined by Eq. (E1) and Eq. (E2), with $\tau \to 0$, can be written as an integral equation,

$$x_j(t) - x_j(0) = \int_0^t v_j dt' + \int_0^t g_j dW(t), \tag{E7}$$

where

$$W(t) = \int_0^t \omega(t')dt', \tag{E8}$$

$$dW(t) = W(t+dt) - W(t). \tag{E9}$$

The second integral in Eq. (E7) is interpreted as a Riemann-Stieltjes-like integral [21],

$$\int_0^t g_j dW(t) = \lim_{N\to\infty} \sum_n^N g_j(\bar{x})[W(t_n) - W(t_{n-1})],$$

where

$$\bar{x} = \lambda x_i(t_{n-1}) + (1-\lambda)x_i(t_n) \tag{E10}$$

with $0 < \lambda < 1$, and $0 = t_0 < \ldots < t_N = t$. Because of the singular nature of the stochastic process $W(t)$, the final result of this integral depends on the chosen value of λ. Each choice provides a different "interpretation" of the Langevin equation [22]: for $\lambda = 1$, the equation is interpreted as "Itô"; for $\lambda = 1/2$, it is interpreted as "Stratonovich"; and for $\lambda = 0$, it is interpreted as "Hänggi-Klimontovich." Each interpretation produces a different FPE. The Stratonovich interpretation leads to Eq. (E5), while for the other interpretations the right-hand side of Eq. (E5) is replaced with

$$-\frac{\partial}{\partial x_j}\left[v_j\rho - D\frac{\partial}{\partial x_i}(g_j g_i \rho)\right] \quad \text{(Itô)}, \tag{E11}$$

$$-\frac{\partial}{\partial x_j}\left[v_j\rho - g_j g_i D\frac{\partial}{\partial x_i}(\rho)\right] \quad \text{(Hänggi)}. \tag{E12}$$

In the specific case of Eq. (1) with $g = (-y, x)$, we have $\partial_i g_i \rho = g_i \partial_i \rho$. Consequently the same FPE is obtained for both the Stratonovich and the Hänggi interpretations. We note that turning off the squeeze in Eq. (1) ($w = 0$) and using either of these interpretations, the FPE becomes

$$\frac{\partial}{\partial t}\rho(x,y,t) = D\left(x\frac{\partial}{\partial y} - y\frac{\partial}{\partial x}\right)^2 = D\frac{\partial^2}{\partial \varphi^2}\rho, \tag{E13}$$

which is clearly the required equation. However, if one uses the Itô prescription, an additional term appears in the FPE, namely, $-D\partial_x(x\rho) - D\partial_y(y\rho)$.

[1] N. G. Van Kampen, Itô versus Stratonovich, J. Stat. Phys. **24**, 175 (1981).

[2] M. Chuchem, K. Smith-Mannschott, M. Hiller, T. Kottos, A. Vardi, and D. Cohen, Quantum dynamics in the bosonic Josephson junction, Phys. Rev. A **82**, 053617 (2010).

[3] C. S. Gerving, T. M. Hoang, B. J. Land, M. Anquez, C. D. Hamley, and M. S. Chapman, Non-equilibrium dynamics of an unstable quantum pendulum explored in a spin-1 Bose-Einstein condensate, Nat. Commun. **3**, 1169 (2012).

[4] B. Misra and E. C. G. Sudarshan, The Zeno's paradox in quantum theory, J. Math. Phys. **18**, 756 (1977).

[5] W. M. Itano, D. J. Heinzen, J. J. Bollinger, and D. J. Wineland, Quantum Zeno effect, Phys. Rev. A **41**, 2295 (1990).

[6] M. C. Fischer, B. Gutiérrez-Medina, and M. G. Raizen, Observation of the Quantum Zeno and Anti-Zeno Effects in an Unstable System, Phys. Rev. Lett. **87**, 040402 (2001).

[7] A. G. Kofman and G. Kurizki, Universal Dynamical Control of Quantum Mechanical Decay: Modulation of the Coupling to the Continuum, Phys. Rev. Lett. **87**, 270405 (2001).

[8] G. Gordon and G. Kurizki, Preventing Multipartite Disentanglement by Local Modulations, Phys. Rev. Lett. **97**, 110503 (2006).

[9] Y. Khodorkovsky, G. Kurizki, and A. Vardi, Bosonic Amplification of Noise-Induced Suppression of Phase Diffusion, Phys. Rev. Lett. **100**, 220403 (2008).

[10] Y. Khodorkovsky, G. Kurizki, and A. Vardi, Decoherence and entanglement in a bosonic Josephson junction: Bose-enhanced quantum-Zeno control of phase-diffusion, Phys. Rev. A **80**, 023609 (2009).

[11] C. Khripkov, A. Vardi, and D. Cohen, Squeezing in driven bimodal Bose-Einstein condensates: Erratic driving versus noise, Phys. Rev. A **85**, 053632 (2012).

[12] E. Boukobza, M. G. Moore, D. Cohen, and A. Vardi, Nonlinear Phase Dynamics in a Driven Bosonic Josephson Junction, Phys. Rev. Lett. **104**, 240402 (2010).

[13] O. Morsch and M. Oberthaler, Dynamics of Bose-Einstein condensates in optical lattices, Rev. Mod. Phys. **78**, 179 (2006).

[14] I. Bloch, J. Dalibard, and W. Zwerger, Many-body physics with ultracold gases, Rev. Mod. Phys. **80**, 885 (2008).

[15] H. Risken, *The Fokker-Planck Equation* (Springer, Berlin, 1984).

[16] W. T. Coffey, Y. P. Kalmykov, and E. S. Massawe, Effective-eigenvalue approach to the nonlinear Langevin equation for the Brownian motion in a tilted periodic potential. II. Application to the ring-laser gyroscope, Phys. Rev. E **48**, 699 (1993).

[17] M. Albiez, R. Gati, J. Fölling, S. Hunsmann, M. Cristiani, and M. K. Oberthaler, Direct Observation of Tunneling and Nonlinear Self-Trapping in a Single Bosonic Josephson Junction, Phys. Rev. Lett. **95**, 010402 (2005).

[18] S. Levy, E. Lahoud, I. Shomroni, and J. Steinhauer, The ac and dc Josephson effects in a Bose-Einstein condensate, Nature **449**, 579 (2007).

[19] P. Kloeden and E. Platenm, *Numerical Solution of Stochastic Differential Equations* (Springer, Berlin, 1992).

[20] CW. Gardiner, *Handbook of Stochastic Methods* (Springer, Berlin, 1985).

[21] P. Hänggi, Stochastic processes. I. Asymptotic behaviour and symmetries, Helv. Phys. Acta **51**, 183 (1978).

[22] I. M. Sokolov, Ito, Stratonovich, Hänggi and all the rest: The thermodynamics of interpretation, Chem. Phys. **375**, 359 (2010).